Journal of Nuclear Materials 89 (1980) 359–371

THE EARLY STAGES OF VOID AND INTERSTITIAL LOOP EVOLUTION IN PULSED FUSION REACTORS

N.M. GHONIEM
School of Engineering and Applied Science, University of California, Los Angeles, California 90024, USA

Received 20 August 1979; in revised form 10 December 1979

A hierarchy of rate equations describing the concentrations of small voids and interstitial loops is used to analyze the effects of radiation pulsing on the early stages of void and interstitial loop evolution. The number of necessary rate equations for the complete description of the clustering process is found to be dependent upon the irradiation time and is obtained by solving an atom conservation equation. Irradiation environments representative of Magnetic Confinement Fusion Reactors of the tokamak-type, Pulsed Heavy Ion Accelerators and Inertial Confinement Fusion Reactors (ICFR's) are considered in this study. At the same average damage rate, it is shown that the high instantaneous atom displacement rate, such as in Pulsed Accelerators or ICFR's, produces high density void and loop clusters of small average sizes. The implications of point defect clustering under pulsed conditions on void nucleation and the embrittlement of the first wall material are discussed.

1. Introduction

The performance of materials in fusion reactors is recognized as a fundamental matter affecting the technical and economic feasibility of fusion power. Radiation effects on the integrity and mechanical behavior of reactor components are therefore important to the designer of fusion reactors. Mechanical properties are known to be strongly influenced by microstructural changes caused by radiation induced defects.

Point defect clustering has been the subject of recent interest [1–9]. This is primarily due to the important role that point defect clusters play in a multitude of radiation induced and enhanced phenomena; such as swelling, creep deformation, embrittlement and loss of ductility. The goal of this investigation is to examine the simultaneous formation of interstitial loops and microvoids in irradiation conditions representative of a range of pulsed fusion reactors.

A detailed rate theory for the homogeneous clustering of point defects has been recently developed by Ghoniem and Cho [8]. In this development, a hierarchy of single rate equations was used to describe the time dependent concentrations of point defect clusters. Aside from the feature of simultaneously describing the two main components of the irradiation produced microstructure, namely interstitial loops and microvoids, the model included size-dependent bias factors and mixed rate reactions (diffusion and surface limited) for computing point defect impingement and emission rates.

The pulsed nature of irradiation in fusion reactors (with the exception of mirror machines) offers an environment where point defect behavior is particularly interesting. Most of the rate processes controlling point defect agglomeration are nonlinear second order reactions (they are functions of products of concentrations). It is expected, therefore, that transient excursions from steady-state behavior can lead to non-recoverable effects on defect size distributions, number densities, average size, nucleation rates and growth behavior. We will briefly present the computational model that is used to describe defect kinetics. One important aspect of this model is the atom conservation principle that determines the necessary number of rate equations. The pulsed irradiation environment will then be described in order to define three reference systems covering a practical range of

pulsed conditions. Results of the calculations for these systems will then be discussed, and conclusions of the work will finally be presented.

2. Computational model

2.1. Basic equations

One of the important considerations in applying the rate theory to the microstructure development during irradiation is the proper determination of the rate constants. While the question of the rate controlling step for point defect interaction with clusters is not conclusively resolved, we assume here that a combination of bulk diffusion and surface reaction will determine the kinetics. Thus, the slower of matrix diffusion and surface reaction rates dictates point defect transport from the matrix to defect clusters. In addition, Wolfer's calculations [10] of point defect diffusion in the drift fields of interstitial loops and cavities were used to determine the size-dependent bias functions. A complete analysis of the rate constants is given in reference [9], and therefore will not be repeated. The point to mention here is that the expressions for the rate constants become strongly non-linear functions of the defect cluster size, which increases the computational requirements for solving the hierarchy of rate equations.

Considering the rates of production and destruction of various defect species, one can derive a consistent set of rate equations for the concentrations of interstitial loop and cavity clusters. This was given in detail in ref. [9], but will be briefly outlined here for convenience.

In constructing the present model, the formation of defect clusters is assumed to occur by the interaction of the randomly migrating point defects and the stationary defect clusters. Since no spatial effects are considered, the mathematical description can be viewed as a point kinetics model. Divacancies are allowed to migrate only to dislocations. The effects of collision cascade collapse on the clustering problem are not treated here, and hence the vacancy and interstitial production rates are taken to be equal. The following rate equations describe the concentrations of the various defect sizes:

$$\mathrm{d}C_\mathrm{v}/\mathrm{d}t = P + K_\mathrm{i}^\mathrm{c}(2)\, C_\mathrm{i}C_{2\mathrm{v}} + (2\gamma_\mathrm{v}^\mathrm{c}(2) - K_\mathrm{v}^\mathrm{c}(2)\, C_\mathrm{v})\, C_{2\mathrm{v}} + \sum_{x=3}^{N_1} (\gamma_\mathrm{v}^\mathrm{c}(x) - K_\mathrm{v}^\mathrm{c}(x)\, C_\mathrm{v})\, C_{x\mathrm{v}} - \sum_{x=3}^{N_1} K_\mathrm{v}^\mathrm{1}(x)\, C_\mathrm{v}C_{x\mathrm{i}} + Z_\mathrm{v}\rho_\mathrm{d}D_\mathrm{v}(C_\mathrm{v}^\mathrm{e} - C_\mathrm{v}) - \alpha C_\mathrm{v}C_1 - K_\mathrm{v}^\mathrm{c}(1)\, C_\mathrm{v}^2 - K_\mathrm{v}^\mathrm{1}(2)\, C_\mathrm{v}C_{2\mathrm{i}}\,, \tag{1a}$$

$$\mathrm{d}C_{2\mathrm{v}}/\mathrm{d}t = \tfrac{1}{2}K_\mathrm{v}^\mathrm{c}(1)\, C_\mathrm{v}^2 + \gamma_\mathrm{v}^\mathrm{c}(3)\, C_{3\mathrm{v}} + K_\mathrm{i}^\mathrm{c}(3)\, C_\mathrm{i}C_{3\mathrm{v}} + \rho_\mathrm{d}D_{2\mathrm{v}}C_{2\mathrm{v}}^\mathrm{e} - K_\mathrm{v}^\mathrm{c}(2)\, C_\mathrm{v}C_{2\mathrm{v}} - K_\mathrm{i}^\mathrm{c}(2)\, C_\mathrm{i}C_{2\mathrm{v}} - \gamma_\mathrm{v}^\mathrm{c}(2)\, C_{2\mathrm{v}} - \rho_\mathrm{d}D_{2\mathrm{v}}C_{2\mathrm{v}}\,, \tag{1b}$$

$$\mathrm{d}C_\mathrm{c}(x)/\mathrm{d}t = K_\mathrm{v}^\mathrm{c}(x-1)\, C_\mathrm{v}C_\mathrm{c}(x-1) - \{K_\mathrm{i}^\mathrm{c}(x)\, C_\mathrm{i} + K_\mathrm{v}^\mathrm{c}(x)\, C_\mathrm{v} + \gamma_\mathrm{v}^\mathrm{c}(x)\}\, C_\mathrm{c}(x) + \{K_\mathrm{i}^\mathrm{c}(x+1)\, C_\mathrm{i} + \gamma_\mathrm{v}^\mathrm{c}(x+1)\}\, C_\mathrm{c}(x+1)\,, \quad 3 \leqslant x \leqslant N_1\,, \tag{1c}$$

$$\mathrm{d}C_\mathrm{i}/\mathrm{d}t = P + K_\mathrm{v}^\mathrm{1}(2)\, C_\mathrm{v}C_{2\mathrm{i}} - K_\mathrm{v}^\mathrm{c}(1)\, C_\mathrm{i}^2 - \alpha C_\mathrm{v}C_\mathrm{i} + 2\gamma_\mathrm{i}^\mathrm{1}(2)\, C_{2\mathrm{i}} - K_\mathrm{i}^\mathrm{1}(2)\, C_\mathrm{i}C_{2\mathrm{i}} - K_\mathrm{i}^\mathrm{c}(2)\, C_\mathrm{i}C_{2\mathrm{v}} - \sum_{x=3}^{N_2} K_\mathrm{i}^\mathrm{1}(x)\, C_\mathrm{i}C_{x\mathrm{i}} - \sum_{x=3}^{N_2} K_\mathrm{v}^\mathrm{c}(x)\, C_\mathrm{i}C_{x\mathrm{v}} - Z_\mathrm{i}\rho_\mathrm{d}D_\mathrm{i}C_\mathrm{i}\,, \tag{1d}$$

$$\mathrm{d}C_{2\mathrm{i}}/\mathrm{d}t = \tfrac{1}{2}K_\mathrm{i}^\mathrm{1}(2)\, C_\mathrm{i}^2 + K_\mathrm{v}^\mathrm{1}(3)\, C_\mathrm{v}C_{3\mathrm{i}} - K_\mathrm{i}^\mathrm{1}(2)\, C_\mathrm{i}C_{2\mathrm{i}} - K_\mathrm{v}^\mathrm{1}(2)\, C_\mathrm{v}C_{2\mathrm{i}} - \gamma_\mathrm{i}^\mathrm{1}(2)\, C_{2\mathrm{i}}\,, \tag{1e}$$

$$\mathrm{d}C_1(x)/\mathrm{d}t = K_\mathrm{i}^\mathrm{1}(x-1)\, C_\mathrm{i}C_1(x-1) + \gamma_\mathrm{v}^\mathrm{1}(x-1)\, C_1(x-1) - \{K_\mathrm{i}^\mathrm{1}(x)\, C_\mathrm{i} + K_\mathrm{v}^\mathrm{1}(x)\, C_\mathrm{v} + \gamma_\mathrm{v}^\mathrm{1}(x)\}\, C_1(x) + K_\mathrm{v}^\mathrm{1}(x+1)\, C_\mathrm{v}C_1(x+1)\,, \quad 3 \leqslant x \leqslant N_2\,. \tag{1f}$$

The variables used in eqs. (1) are defined in table 1. For a detailed discussion of the reaction rate constants and diffusion coefficients, the reader is referred to the work of Ghoniem and Cho [8,9].

2.2. Species conservation

One of the important questions that arise when one attempts to solve kinetic equations such as those given by (1), is how many equations are good enough for an accurate solution? Various investigators [4,7] pointed out this particular difficulty. Results of rather lengthy computations can be misleading if one solves for the wrong number of equations [7]. In order to overcome this inconvenience, we utilized a simple atom conservation principle that describes a

Table 1
Definition of the variables of eq. (1)

Variable	Definition	Units
$C_{v,i}$	Vacancy/interstitial concentration	at/at
$C_{2v,2i}$	Divacancy/diinterstitial concentration	at/at
x	Number of atoms/vacancies in a loop/cavity	
$C_{c,l}(x)$	Size x cavity/loop concentration	at/at
P	Point defect production rate	at/at · s
$\nu_{v,i}$	Vacancy/interstitial vibrational frequency	s^{-1}
α	Recombination coefficient $\alpha = 48\nu_i \exp(-E_i^m/kT)$	s^{-1}
$Z_{v,i}$	Vacancy/interstitial–straight dislocation bias factors	
ρ	Straight dislocation density	m^{-2}
D_{2v}	Divacancy diffusion coefficient $D_{2v} = \nu_v a^2 \exp(-E_{2v}^m/kT)$	m^{-2}
C_{2v}^e	Divacancy thermal concentration $C_{2v}^e = 6 \exp(-(2E_v^f - E_{2v}^B)/kT)$	at/at
N_1	Number of equations for vacancy clusters	
N_2	Number of equations for interstitial clusters	
$K_{v,i}^{c,l}(x)$	Impingement frequencies of vacancies/interstitials on a size x cavity/loop	s^{-1}
$\gamma_v^c(x)$	Vacancy emission rate from cavities	s^{-1}
$\gamma_{v,i}^{c,l}(2)$	Divacancy/diinterstitial thermal dissociation rates	s^{-1}

global quantity defined as the *net* number of interstitial atoms in loops.

We will demonstrate here the atom conservation principle by only considering atoms in interstitial loops. It will be shown that this is a reasonable choice, since the interstitial clustering process will be demonstrated to be much faster than the corresponding void formation. The net integrated number of atoms in interstitial loops per cubic meter is obtained by integrating the rates of atomic deposition in all loops. This is given by

$$\Omega^{-1} \int_0^{t^*} \left\{ \sum_{x=2}^{N_1} [K_i^1(x-1,t')\, C_i C_1(x-1,t') - K_v^1(x,t')\, C_v C_1(x,t')] - 2\gamma_i^1(2,t')\, C_1(2,t') \right\} dt' , \quad (2)$$

where the first term between the brackets represents the rate of interstitial atom impingement on cluster size $(x-1)$, the second term is the rate of vacancy flow into size (x) and the last term is the rate of diinterstitial cluster dissociation. The expression given by eq. (2) gives the required number of atoms at time t^*. On the other hand, if we consider the interstitial loop size distribution at the time t^*, the total number of atoms per cubic meter is obtained by summing over all cluster concentrations, and is therefore given by

$$f(t^*) = \Omega^{-1} \sum_{x=2}^{N_1} x C_1(x,t^*) . \quad (3)$$

Now we can define a relative error (ϵ) by subtracting eq. (3) from (2) and normalizing to the total interstitial atom concentration. The number of necessary rate equations to be solved at the time t^* should satisfy the relationship

$$\frac{1}{f(t^*)} \left[\int_0^{t^*} \left\{ \sum_{x=2}^{N_1} [K_i^1(x-1,t')\, C_i C(x-1,t') - K_v^1(x,t')\, C_v C_1(x,t')] - 2\gamma_i^1(2,t')\, C_1(2,t') \right\} dt' - 1 \right] \leqslant \epsilon . \quad (4)$$

Here, we choose the number of equations, N_1, in order to minimize the relative error ϵ. To illustrate this point, we will consider the system of eqs. (1) for an irradiation environment typical of tokamak designs. Parameters of table 2 are used in the calculations for a 316 stainless steel first wall. For this reference case we used the values: $P = 10^{-6}$ dpa/s, $\rho_d =$

Table 2
Parameters for 316 stainless steel

Parameter	Symbol	Numerical value	Units	Reference
Interstitial–interstitial combinatorial number	$C_i^I(1)$	84		[4]
Vacancy–vacancy combinatorial number	$C_v^c(1)$	84		[4]
Vacancy migration energy	E_v^m	2.24×10^{-19}	J	[11]
Interstitial migration energy	E_i^m	3.2×10^{-20}	J	[11]
Vacancy formation energy	E_{vf}^f	2.56×10^{-19}	J	[11]
Interstitial formation energy	E_i^f	6.54×10^{-19}	J	[11]
Lattice parameter	a	3.63×10^{-10}	m	[4]
Interstitial vibrational frequency	ν_i	5×10^{12}	s^{-1}	[7]
Vacancy vibrational frequency	ν_v	5×10^{13}	s^{-1}	[7]
Divacancy migration energy	E_{2v}^m	1.44×10^{-19}	J	[12]
Divacancy binding energy	E_{2v}^B	4×10^{-20}	J	[12]
Trivacancy binding energy	E_{3v}^B	1.22×10^{-19}	J	[12]
Vacancy–dislocation bias factor	Z_v	1.0		[11]
Interstitial–dislocation bias factor	Z_i	1.08		[11]
Surface energy	g	1	J/m^2	[11]

10^{13} m/m^2, $T = 723$ K and the pulse duration longer than 10 s.

Consider the results of the computations for the reference conditions. Two different systems with an initial number of 20 equations for interstitial loops were studied. In system 1, N_1 was dynamically incremented by 5 equations at every output step. On the other hand, the number of equations in system 2 was increased by 5 up to a maximum of 40, and then was held constant until the end of irradiation. Fig. 1 shows N_1 and ϵ as functions of the irradiation time for both systems. It is obvious that the error for the two systems should be identical up to 2 s, since the number of equations was increased by the same amount. It is interesting to notice, however, that while the error is always small for system 1 ($-1\% \leqslant \epsilon \leqslant +2\%$) during the entire period, it switches to a positive value after 2 s and then increases rapidly. One of the boundary conditions used here as well as in other investigations [4,7] is that the concentration of the $N_1 + 1$ interstitial cluster is zero. When N_1 is fixed to 40 in the second system after 2 s, significant errors are introduced in the calculations as can be seen from fig. 1. The concentration of interstitial clusters containing 41 atoms should in reality increase, pass through a maximum and then decrease to its quasi-equilibrium value as irradiation time proceeds. Since the number of equations is automatically increased in the first system, the buildup and decay of successively larger cluster sizes is automatically taken care of by dynamically increasing the number of equations, and therefore the error is kept at a minimum.

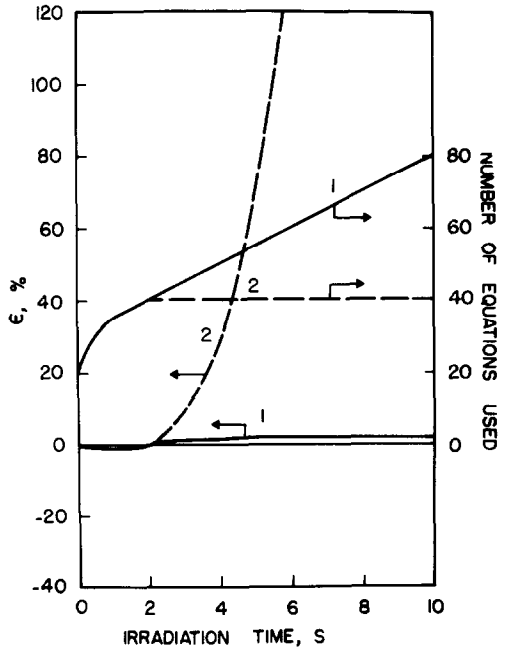

Fig. 1. Relative error and number of single rate equations as functions of irradiation time. (1) Dynamic incrementing. (2) Incrementing up to a maximum of 40 equations.

Table 3
Parameters of the pulsed fusion systems

Concept	T_{on} (s)	T_p (s)	P (dpa/s)
Magnetic Confinement Fusion Reactor	224	245	10^{-6}
Simulation Facility (Heavy Ion Pulsed Accelerator)	10^{-3}	1	10^{-3}
Inertial Confinement Fusion Reactor (ICFR)	10^{-6}	1	1

3. Description of the pulsed irradiation environment

Generally speaking, the behavior of microstructural components such as voids and interstitial dislocation loops is dictated by the many material and irradiation variables. Of particular interest for damage analysis of pulsed fusion reactors, however, are the on-time (T_{on}), the pulse period (T_p) and the damage rate during the irradiation pulse (P). In pulsed fusion reactors damage will be generated only during the irradiation pulse, after which the first wall material relaxes (anneals) until the end of T_p.

For a meaningful comparison of the effects of radiation pulsing on the behavior of the microstructure in various reactor concepts, three pulsed systems are chosen here to represent a spectrum of fusion reactor designs with the same *average* displacement rate. Various proposed designs for pulsed fusion reactors were found to experience roughly the same average damage rate in the bulk of the first wall material [13]. Moreover, choosing the average dose rate as a fixed basis of comparison will eliminate any results due to variations in the average damage rate and will more clearly bring about the special effects of radiation pulsing. The question of what happens when the average damage rate is accelerated (such as in simulation facilities) is not addressed in this study. A description of the three pulsed fusion systems is shown in table 3, where the pulsing characteristics of two extreme concepts (tokamak and ICFR) are shown along with those of a pulsed accelerator having intermediate parameters. The tokamak conditions are those of a recent magnetic fusion design [14], while the other two cases are intended to encompass intermediate [15] (10^{-3} dpa/s) and high [16] (1 dpa/s) displacement rates

Throughout the calculations, the material parameters of table 2 are used. Also, an irradiation temperature of 723 K and an initial dislocation density of 10^{13} m/m^3 are chosen to represent a reasonable reference case that is typical of reactor first wall conditions. Since this study is directed towards a detailed understanding of the initial stages of clustering (irradiation time up to 10 s), only 10 equations are used for vacancy clusters. This number of equations was found to be sufficient for the short times considered here because of the slow vacancy clustering process [8].

4. Results of the calculations

4.1. Tokamak reactors

The time evolution of interstitial loops and microvoids at 723 K for the typical tokamak irradiation conditions described above is shown in fig. 2. For times less than $\sim 10^{-4}$ s, the concentrations of both single vacancies and interstitials increase linearly with time. Point defect losses are insignificant during such short intervals. At later times, interstitial diffusion to straight dislocations becomes important, and then recombination dominates after ~0.1 s. Only, a small fraction of interstitials (~0.8%) contributes to the nucleation and growth of the interstitial loops. It should be also noted that the concentrations of microvoids is extremely low during the period of interest (10 s). The average interstitial loop size ($\bar{x}$) is shown in fig. 3, and the growth speed of the average size, $d\bar{x}/dt$ (atoms/s), is depicted in fig. 4. The figures indicate that after an initial transient, the average

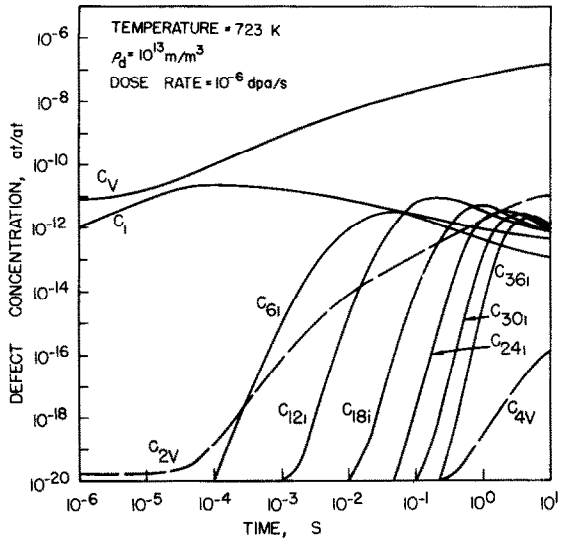

Fig. 2. Concentration of vacancy clusters and small interstitial loops as functions of irradiation time for the tokamak conditions.

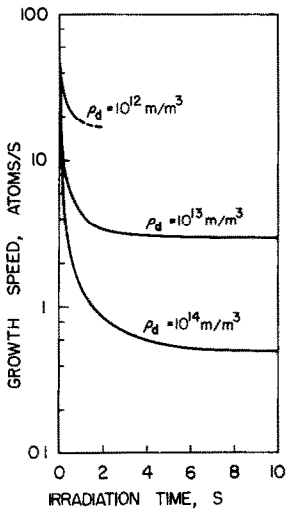

Fig. 4. Growth speed of the average loop size ($d\bar{x}/dt$) in tokamak irradiation environments.

loop size increases almost linearly with time, while the growth speed drops to a constant value. It can be seen from figs. 3 and 4 that the initial dislocation density has substantial effects on the growth properties of the nucleating interstitial loops. A higher initial dislocation density (produced by cold working the first wall material) will slow down the growth kinetics resulting in a smaller growth speed and hence average size. The size distribution of microvoids is shown in fig. 5. Up to 10 s of irradiation, the concentrations are shown to be continuously decreasing functions of size. The concentrations of large size vacancy clusters are extremely low. This is consistent with the relatively longer incubation period for void nucleation.

Over the time period of the calculations (10 s), tokamak conditions are equivalent to steady-irradiation only during the first cycle. Investigating the behavior of loops during the remainder of the first on-time and the effects of multiple pulses is beyond

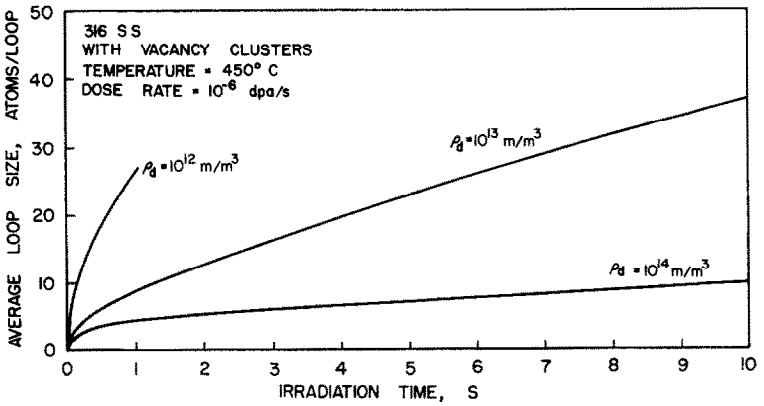

Fig. 3. Average interstitial loop size for different initial dislocation densities corresponding to the tokamak irradiation environments.

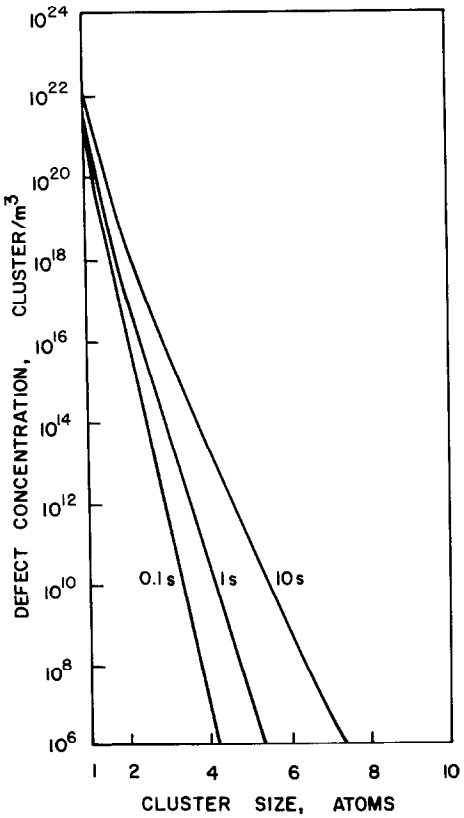

Fig. 5. Microvoid size distributions in tokamak irradiation environments.

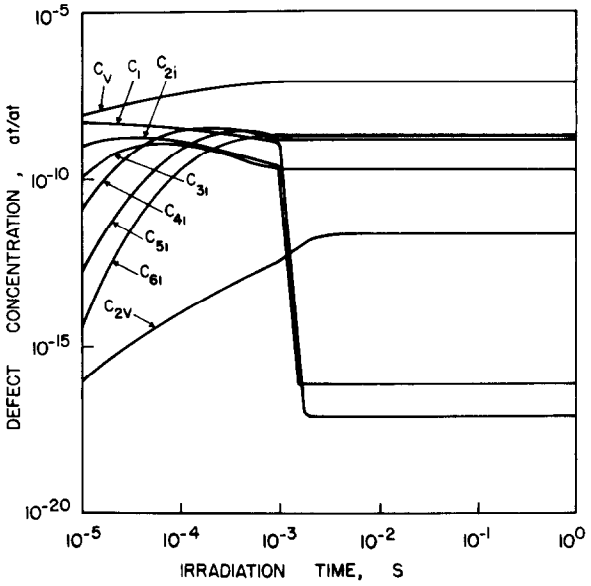

Fig. 6. Defect cluster concentrations in pulsed accelerator irradiation conditions ($P = 10^{-3}$ dpa/s during 10^{-3} s and $T_p = 1$ s).

the computational capabilities of the present technique. In order to look at these specific effects, Ghoniem and Sharafat [17] have developed an alternate continuum solution to the clustering problem. Their technique, which is computationally advantageous when one is interested in long-term behavior of clusters, is based on a numerical descritization technique to the Fokker–Planck equation.

4.2. Pulsed accelerators

The time evolution of interstitial loops, single vacancies and divacancies during the first irradiation cycle of the pulsed accelerator described in the previous section is shown in fig. 6. The single interstitial concentration peaks at ~10 μs, then decreases due to recombination with vacancies and the creation of diinterstitials and larger size loops. Right after the irradiation pulse, point defect generation is discontinued, and fast diffusion of single interstitials to dislocations results in a sharp decrease in their concentration. The concentration of diinterstitials also decreases rapidly after the pulse, only by the dissociation into single interstitials (no migration). All other defect cluster concentrations remain at a quasi-steady state until the start of the next pulse. Since the thermal annealing rate is very small, and defect clusters are immobile, the concentrations remain almost constant until the end of the cycle. The forward and backward reaction rates are approximately balanced until the start of the next cycle.

The fractional concentrations of single and diinterstitials determined by pure thermodynamic considerations are extremely low. In the present case of stainless steel at 723 K, the thermodynamic equilibrium concentration of single interstitials is $\sim 3.6 \times 10^{-29}$ at/at, and the corresponding concentration of diinterstitials is $\sim 2.6 \times 10^{-49}$ at/at. The dynamic calculations, however, result in quasi-steady state concentrations during the off-time that are determined by the approximate balance of forward and backward reaction rates. When the irradiation source is absent, the

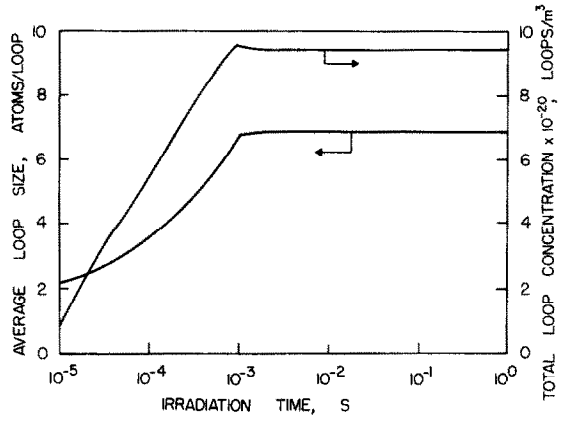

Fig. 7. Average loop size and total concentration of loops in the pulsed accelerator case.

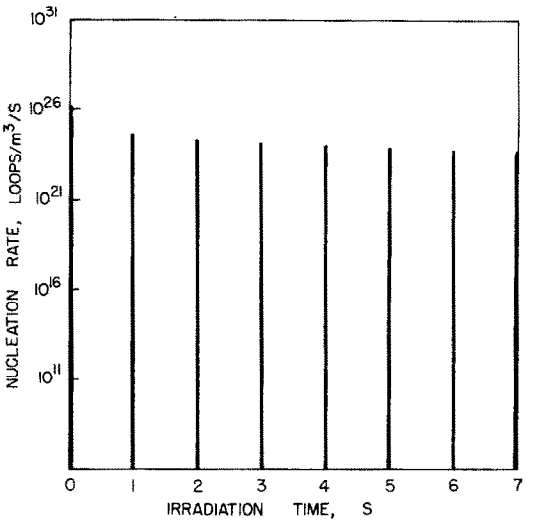

Fig. 8. Interstitial loop nucleation rate in a sequence of pulses of 1 ms duration.

concentration of diinterstitials is roughly determined by the balance between the formation rate due to single vacancies impinging on triinterstitials, and the dissociation rate of diinterstitials. Therefore, the quasi-steady state concentration during the off-time is approximately given by:

$$C_{2i}^{QSS} \simeq \left(\frac{K_v^1(2)\, C_v^{QSS}}{\gamma_i^1(2)}\right) C_{3i}^{QSS} \simeq 7.0 \times 10^{-17} \text{ at/at.} \quad (5)$$

Similarly, the quasi-steady state single interstitial concentration is determined by

$$C_i^{QSS} \simeq \left(\frac{2\gamma_i^1(2)}{\alpha C_v^{QSS} + Z_i \rho_d D_i}\right) C_{2i}^{QSS}$$

$$\simeq 7.7 \times 10^{-18} \text{ at/at .} \quad (6)$$

The concentrations of single and diinterstitials during the off-time are therefore orders of magnitudes larger than their thermodynamic equilibrium values.

The average loop size and the total concentration of loops as functions of irradiation time for an entire period is shown in fig. 7. It is interesting to notice that the loop growth and the increase in loop concentration occurs almost entirely during the on-time. After about 1 ms, the loop concentration reaches the very high value of $\sim 10^{21}$ loops/m^3, and remains relatively constant until the start of the next pulse. Defining the loop nucleation rate as the total number of loops formed per unit volume per second, we find that the nucleation rate is very high during the short on-time, and is almost zero during the off-time. This is demonstrated for seven consecutive pulses in fig. 8. The nucleation rate is on the order of $\sim 10^{24}$ loops/m^3 · s and is shown as sharp impulses which occur only during the short on-time of 1 ms.

The interstitial loop size distributions at four different irradiation times are shown in fig. 9. The size distribution is almost identical for 0.1 and 1 s, since the distribution is mainly established during the short damage interval. The evolution of loops is thus negligible during the annealing period at 723 K. After the first pulse, the distribution peaks around 6 interstitials. The peak size then moves to 22 interstitial atoms and the distribution becomes much broader by the end of 7 pulses.

The fractional concentrations of small size vacancy clusters are shown in fig. 10 as functions of time during the first pulse. One of the major differences between vacancy and interstitial clustering is the much slower transients associated with vacancies. When the irradiation is shut off, single vacancies diffuse very slowly to sinks, thereby maintaining a relatively high concentration during the off-time. Thus, the vacancy supersaturation ($S = C_v/C_v^e$) has the high value of $\sim 1.14 \times 10^4$ during the off-time. This large supersaturation of vacancies promotes the vacancy clustering process, even though the irradiation source

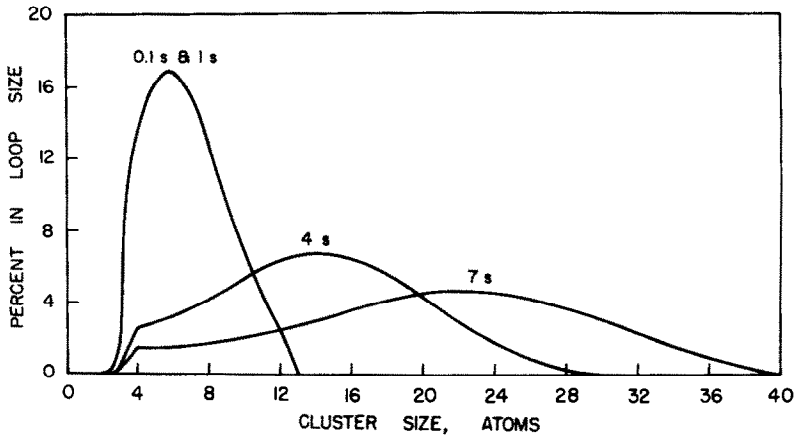

Fig. 9. Interstitial loop size distributions at various irradiation times for the pulsed accelerator.

is turned off. The vacancy clustering process is clearly shown in fig. 10. It has to be noted, however, that the thermal vacancy emission rate is negligible when compared to the vacancy impingement rate at 723 K. At higher temperatures, vacancy clustering is expected to proceed at a much slower rate due to thermal vacancy emission.

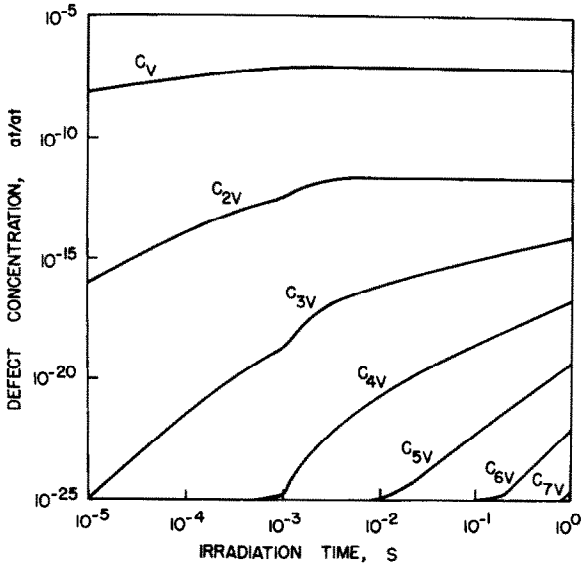

Fig. 10. The fractional concentrations of small size vacancy clusters (microvoids) during one accelerator pulse.

4.3. Inertial Confinement Fusion Reactors

Point defect clustering in ICFR conditions occurs during a very short time (1 μs), and is affected by very high point defect supersaturation ratios resulting from the high atomic displacement rate ($P = 1$ dpa/s). The evolution of interstitial loops during the first pulse is shown in fig. 11. Due to the constant high point defect production rate during the damage pulse, the concentrations of defect clusters increase steadily

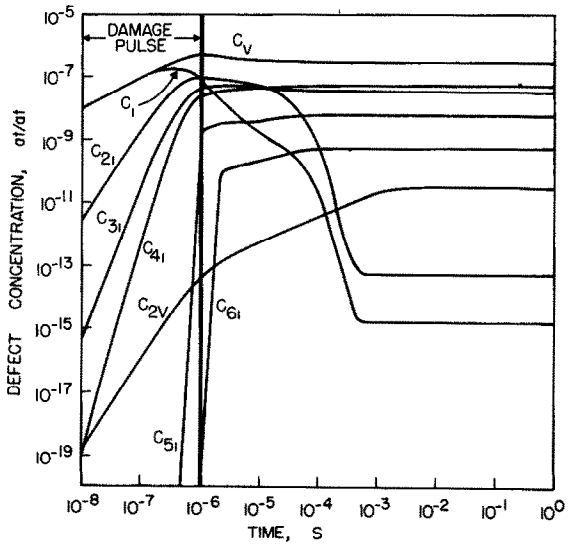

Fig. 11. Point defect cluster evolution during one ICFR pulse.

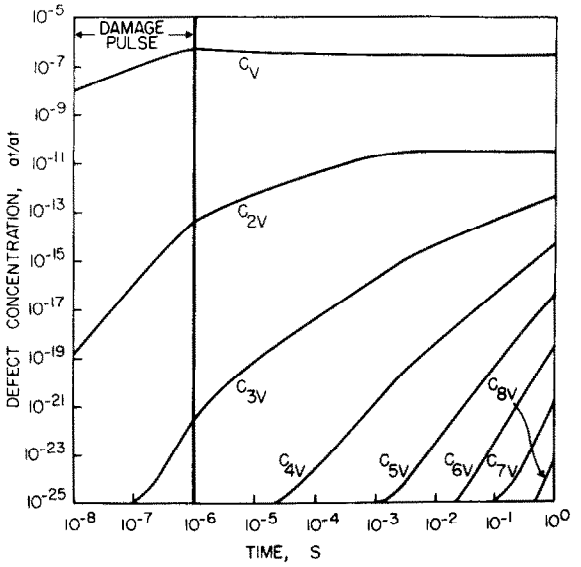

Fig. 12. Microvoid evolution in ICFR irradiation conditions.

until the end of the on-time. Immediately after the damage pulse, single interstitials and diinterstitials decay to their dynamic equilibrium concentrations within ~1 ms. As a result of the very high displacement damage rate during the pulse, the absolute fractional concentrations of defect clusters are shown to be much higher than the previous two cases (compare fig. 11 to figs. 2 and 6). The corresponding microvoid evolution is shown in fig. 12, where the much longer microvoid relaxation times are clearly illustrated. Fig. 13 depicts the effect of single interstitials on the evolution of interstitial loops during the third and ninth periods. The dotted lines represent the size distributions at the end of the on-time. During the off-time, diinterstitials dissociate into single interstitials, which in turn impinge on larger interstitial clusters resulting in their growth. Thus, the loop distribution moves a small amount towards larger sizes with each pulse as shown in fig. 13.

5. A comparison between the pulsed irradiation systems

In this section, we will investigate the effects of radiation pulsing on some of the major parameters describing the microstructure evolution. During the relatively short irradiation period considered in the tokamak calculations (10 s), the irradiation source was not interrupted, and therefore the results represent steady-irradiation within this time interval. The tokamak reactor will be regarded as the reference steady-irradiation case, and the effects of beam

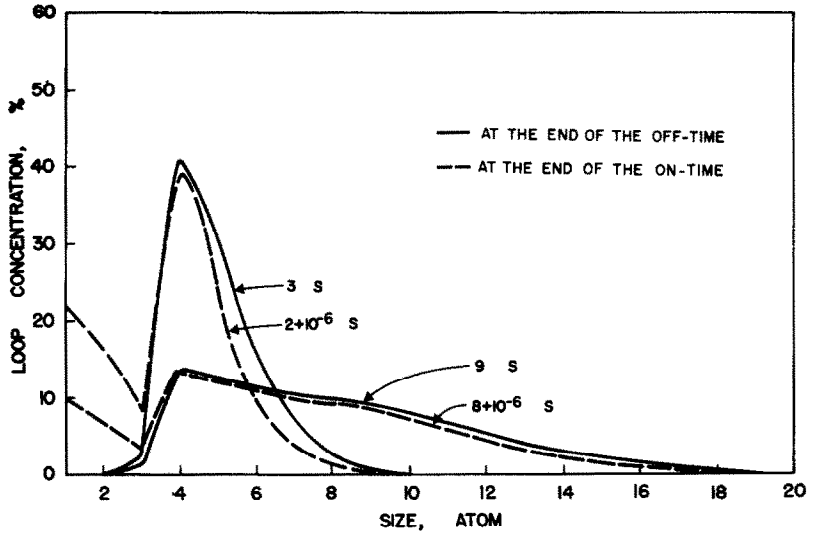

Fig. 13. Interstitial loop size distributions for the third and ninth pulses.

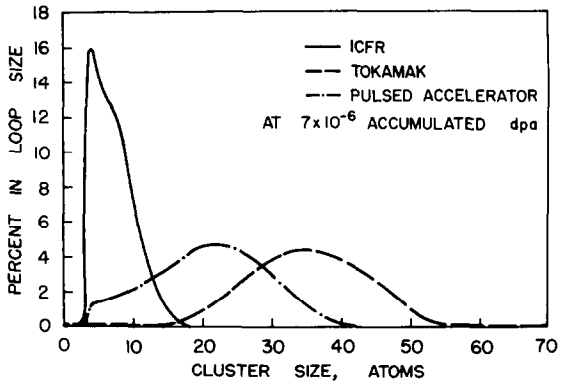

Fig. 14. Interstitial loop size distributions at an equivalent dose of 7×10^{-6} dpa in the three pulsed systems.

pulsing on the behavior of the microstructure will be explored by comparing to the tokamak results.

The interstitial loop size distributions for the three cases are depicted in fig. 14 after an accumulated dose of 7×10^{-6} dpa. It is noted that the size distribution is non-symmetrical for the highly pulsed reactor (ICFR) and approaches a symmetrical shape for the steady-irradiation reactor (tokamak). The peak size is 4 interstitials for the ICFR, 21 for the pulsed accelerator and 34 for the tokamak. A comparison of the average loop size for the 3 systems is given in fig. 15. While the average loop size for the tokamak increases linearly after an initial transient, the size develops in a step function fashion for the other two pulsed sys-

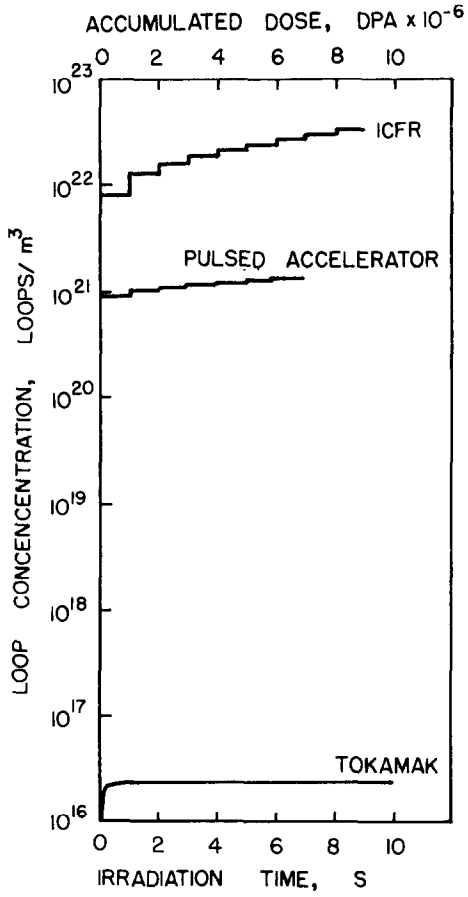

Fig. 16. Time dependence of the loop concentrations for the three equivalent pulsed systems.

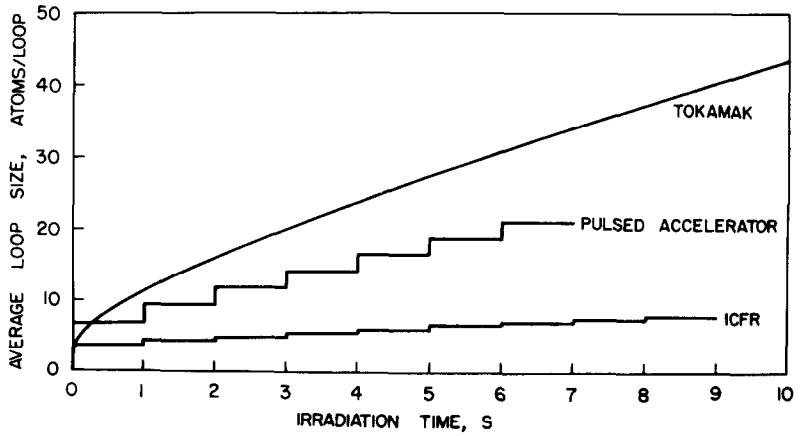

Fig. 15. Average loop size as a function of irradiation time for the three pulsed systems.

tems. It is interesting to note that the average and peak sizes are identical only for the tokamak and the pulsed accelerator. The total loop concentrations are shown as functions of irradiation time and accumulated dose in fig. 16. The loop concentration is shown to increase at a much higher rate in the two pulsed systems when compared to the steady-irradiation tokamak. After an irradiation period of 10 s, the loop concentration is about 10^{16} loops/m^3 for the tokamak reactor, 2×10^{21} loops/m^3 for the pulsed accelerator and 4×10^{22} loops/m^3 for the ICFR.

The simultaneous formation of microvoids is also examined in this section. The calculations indicate that in ICF conditions, the diinterstitial formation rate is faster than the point defect mutual recombination rate due to the high mobility and concentration of single interstitials. This reduces the probability of vacancy–interstitial recombination, and thereby increases the vacancy supersaturation in the first wall of the ICFR. By the end of the on-time, 97% of point defects recombine in the pulsed accelerator and the tokamak cases, and only 67% recombine in the ICFR. The vacancy supersaturation is thus increased in the ICFR, enhancing microvoid formation. Fig. 17 shows the microvoid concentrations (up to a cluster of 10 vacancies) as functions of the irradiation time. Although some of the microvoids dissolve during the annealing period, the damage produced during each pulse results in large discontinuous additions to the total void population. After 7 s, the total microvoid concentration is $\sim 2 \times 10^{19}$ voids/m^3 for the ICFR and $\sim 10^{18}$ voids/m^3 for both the pulsed accelerator and tokamak systems.

As an application of the present calculations, we will consider the clustering effects on the tensile properties of the irradiated material. The irradiation induced changes in tensile properties can be partly attributed to the impedence of dislocation motion by small homogeneously distributed point defect clusters [18]. The increment in the yield stress due to the formation of the small defect clusters is given by an equation of the following form [19]:

$$\Delta\sigma_{\text{Loops}} = Gb\bar{d}\, n_{\text{L}}^{2/3}/\beta\,, \tag{7}$$

where G = shear modulus, b = Burgers vector, $\bar{d}$ = average loop diameter, n_{L} = loop number density and β = a constant. Using the number densities and average sizes from the previous sections, the ratio of the yield stress increment due to irradiation after 10 s is given by:

$$\Delta\sigma^{\text{ICFR}}/\Delta\sigma^{\text{tokamak}} \approx 6739\,. \tag{8}$$

Thus, plastic instability can occur at lower strains in the highly pulsed systems when compared to the steady-irradiation facilities. However, periodic annealing of the defect clusters could be one method of alleviating this particular problem.

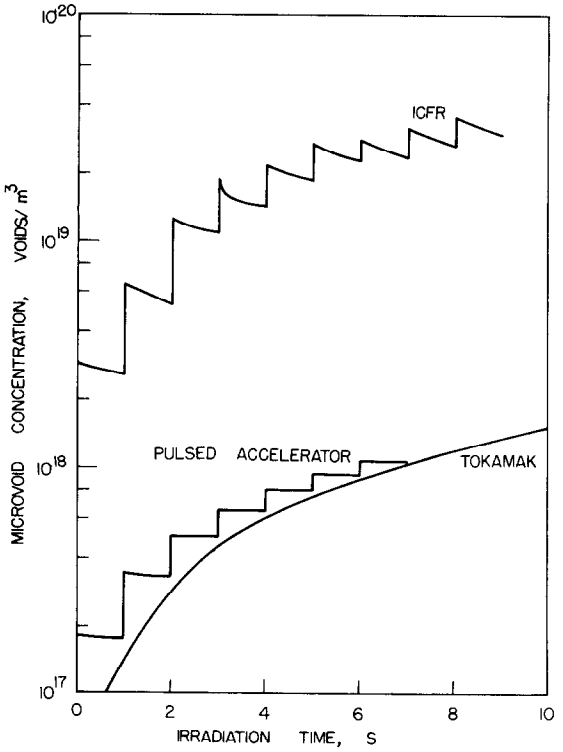

Fig. 17. Microvoid concentrations as functions of irradiation time.

6. Conclusions

The evolution and kinetic behavior of the microstructures (interstitial loops and microvoids) of pulsed fusion reactor first walls have been shown to be strongly dependent on the duration, frequency and magnitude of the irradiation pulse. The following conclusions summarize the major findings of the present work:

(1) An atom conservation equation is necessary to determine the required number of rate equations at any point in time.
(2) A high initial dislocation density (such as that produced by cold working the first wall) slows down the clustering kinetics of point defects.
(3) Interstitial atom clustering is a much faster process when compared to vacancy clustering.
(4) At intermediate temperatures (~723 K), where vacancy annealing is negligible, interstitial atom clustering occurs only during the on-time, while vacancy agglomeration proceeds throughout the entire cycle.
(5) The interstitial loop size distribution in highly pulsed reactors (ICFR's) is narrow and peaked around small size loops. The distribution is much broader in reactors with long burn cycles.
(6) Intense irradiation pulsing (ICFR's) produces small size defect clusters of high density.
(7) In ICFR's, the formation of a high density of small size point defect clusters can result in a large increase in the yield stress of the first wall material leading to probable plastic instabilities at lower strains.
(8) The high concentration of single interstitials in the ICFR case is found to enhance the diinterstitial nucleation rate which reduces point defect mutual recombination. Consequently, the vacancy supersaturation is increased resulting in large microvoid concentrations. The higher void concentration in pulsed systems is in qualitative agreement with the recent experimental data of Powell and Odette [20].

Acknowledgements

The author is grateful to David Cho for his assistance with the calculations. This research was supported by the National Science Foundation through Grant No. ENG78-05413.

References

[1] L.M. Brown, A. Kelly and R.M. Mayer, Phil. Mag. 19 (1969) 721.
[2] M. Kiritani, J. Phys. Soc. Japan 35 (1973) 95.
[3] M. Koiwa, J. Phys. Soc. Japan 37 (1974) 1532.
[4] M.R. Hayns, J. Nucl. Mater. 56 (1975) 267.
[5] M.R. Hayns, J. Nucl. Mater. 59 (1976) 175.
[6] B.O. Hall and D.I. Potter, in: Proc. 9th Intern. Symp. on Effects of Radiation on Structural Materials, Richland, WA, 1978.
[7] R.A. Johnson, J. Nucl. Mater. 75 (1978) 77.
[8] N.M. Ghoniem and D.D. Cho, Phys. Status Solidi (a) 54 (1979).
[9] N.M. Ghoniem and D.D. Cho, Univ. of Calif. Eng. Report UCLA-ENG-7845 (1978).
[10] W.G. Wolfer and M. Ashkin, J. Appl. Phys. 46 (1975) 547.
[11] N.M. Ghoniem and G.L. Kulcinski, Radiation Effects 41 (1979) 81.
[12] A.C. Damask and G. Dienes, Phys. Rev. 120 (1960) 99.
[13] N.M. Ghoniem and G.L. Kulcinski, Univ. of Wisconsin Fusion Report UWFDM-311 (1979).
[14] B. Badger et al., Univ. of Wisconsin Fusion Report UWFDM-330 (1979).
[15] T.M. Williams, J. Nucl. Mater. 79 (1979) 28.
[16] R.W. Conn et al., Univ. of Wisconsin Fusion Report UWFDM-220 (1977).
[17] N.M. Ghoniem and S. Sharafat, J. Nucl. Mater. to be published.
[18] D.R. Harries, J. Nucl. Mater. 82 (1979) 2.
[19] K.H. Westmacott, Phil. Mag. 14 (1966) 239.
[20] R.W. Powell and G.R. Odette, J. Nucl. Mater. 85/86 (1979) 695.